Journal of Organometallic Chemistry, 478 (1994) 189–196

The rearrangement pathway in $[Cp_2Mo_2(CO)_4(RC{\equiv}C{-}CR_2)]^+$ cations: an extended Hückel molecular orbital and Bürgi-Dunitz trajectory study

Luc Girard [a], Philippa E. Lock [a], Hani El Amouri [b] and Michael J. McGlinchey [a]

[a] *Department of Chemistry, McMaster University, Hamilton, Ont. L8S 4M1 (Canada)*

[b] *Ecole Nationale Supérieure de Chimie de Paris, 11, rue Pierre et Marie Curie, 75231 Paris Cedex 05 (France)*

(Received October 6, 1993; in revised form December 17, 1993)

Abstract

The fluxional behavior of metal cluster cations of the type $[Cp_2Mo_2(CO)_4(RC{\equiv}C{-}CR'R'')]^+$ has been widely studied by variable-temperature NMR techniques, and a mechanism involving migration of the carbocationic center between the organometallic vertices has been proposed. In this report, the suggested mechanism has been investigated by means of extended Hückel molecular orbital calculations (EHMO), and allows the evaluation of the lowest energy pathway by which this process may occur. These computations are supplemented by a Bürgi–Dunitz trajectory analysis of 11 X-ray crystal structures of such cations which yields a series of "snapshots" of the migration process. Together the EHMO and trajectory approaches give a remarkably complete picture of the molecular dynamics of such molecules.

Key words: Bürgi–Dunitz trajectory study; Extended Hückel theory; Molybdenum clusters; Rearrangements

1. Introduction

1.1. Criteria for the characterization of fluxional processes

Nowadays, the complete elucidation of a fluxional process generally requires: (a) an X-ray crystal structure to establish the ground-state molecular geometry; (b) the unambiguous attribution of the NMR resonances in the limiting low-temperature spectrum; (c) the identification of the nuclei which undergo site exchange—often achieved directly by means of magnetization transfer techniques; (d) evaluation of the activation energy barrier(s) for the exchange process(es) either by simulating the peak coalescence pattern or by 2D-exchange experiments; and (e) comparison of the experimental activation energies with calculated values of the steric and/or electronic contributions to the barrier obtained by means of molecular modeling and molecular orbital methods, respectively. Such calculational approaches towards evaluating the energy requirements of fluxional processes require that one select a geometrically viable mechanistic pathway through which the rearrangement can occur. Clearly, it would be advantageous if one could experimentally establish the actual trajectory followed by the migrating group.

1.2. The Bürgi-Dunitz trajectory model

In recent years, the powerful concepts developed by Bürgi and Dunitz [1] have proven to be valuable additions to the arsenal of those who wish to gain an understanding of molecular dynamics. It has been demonstrated that a succession of static X-ray structures can give information about the dynamics of a reaction. In their now classic studies Bürgi and Dunitz showed, for example, that a series of crystal structures of systems containing both a nucleophile and an organic carbonyl group could be used to obtain the trajectory of approach of the two reagents [2]. It is clear from these data not only that the nucleophile attacks along a line making an angle of approximately 105° to the C=O bond but also that the trigonal planar sp^2 carbon atom is gradually transformed into a tetrahedral centre. The significance of these observations for mechanistic organic chemistry is profound, and it was soon exploited by Baldwin to rationalize the favor-

Correspondence to: Professor M.J. McGlinchey.

0022-328X/94/$7.00
SSDI 0022-328X(94)24436-M

able or unfavorable nature of many ring-closure processes [3].

Another beautiful result from Dunitz's laboratory [4] showed how the distribution of crystal structures of more than 60 $(C_6H_5)_3P-X$ fragments in many different environments can be related to the "two-ring flip" mechanism by which these chiral propeller-like moieties can undergo racemization. In this process all three phenyl rings do not rotate at the same rate nor in the same direction, and this phenomenon should be reflected in the crystallographic results which capture a series of snapshots of the Ph_3P fragment in different environments. This crystallographically derived picture of the stereoisomerization pathway is complemented by force field calculations and variable-temperature NMR data on related Ar_3CH systems which also favor the "two-ring flip" mechanism [5–8].

The ideas of Bürgi and Dunitz have been elegantly extended into the organometallic arena by Crabtree and Lavin [9]; in their study it was shown that carbonyl migration between two metal atoms proceeds via a trajectory in which a linear terminal ligand proceeds through a series of increasingly more bent semi-bridging structures to a symmetrically bridging situation.

We now describe how the use of a combination of NMR, extended Hückel molecular orbital (EHMO) and Bürgi–Dunitz trajectory data allows one to obtain a relatively complete picture of the mechanism of migration of a vinylidene moiety over the surface of a Mo_2C triangle.

2. Results and Discussion

2.1. *The fluxional behavior of cluster cations, $[M_2L_n(H-C\equiv C-CH_2)]^+$*

The original impetus for these studies was Seyferth's work on $[Co_3(CO)_9C-CR_2]^+$ cations for which the bent structure **1a** was proposed rather than the more symmetrical isomer **1b** with its pseudo-threefold axis [10].

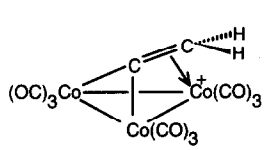

1a

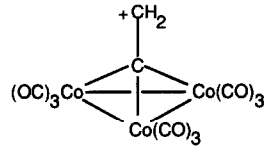

1b

EHMO calculations by Schilling and Hoffmann [11] provided a rationale for the favored structure **1a**; they examined the frontier orbital interactions between a $[Co_3(CO)_9]^{3+}$ triangle and a vinylidene fragment,

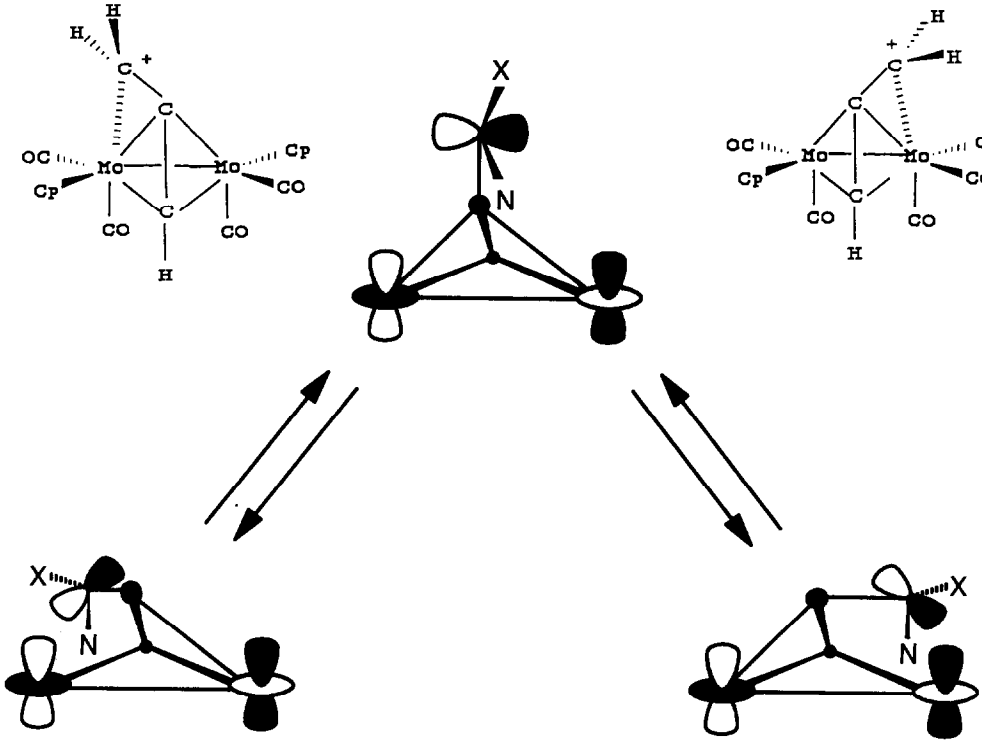

Fig. 1. Antarafacial migration of an α-methylene group between metal centers in a tetrahedral cluster; note how the exo (X) and endo (N) substituents maintain their relative positions.

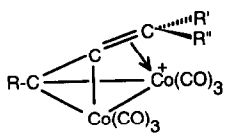

2

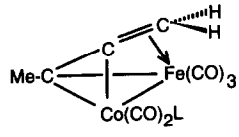

3

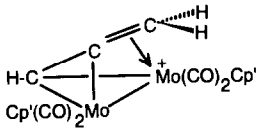

4

$[C{=}CH_2]^{2-}$, and were able to show that the C_s isomer **1a** is energetically markedly preferred over the pseudo-C_{3v} structure **1b**. One can readily envisage that, by allowing the sp^2-hybridized α-carbon to lean towards a cobalt vertex, the vacant p orbital on carbon can accept electron density from a filled metal d orbital. The net result is not only enhanced stabilization of the cationic center, via delocalization of the positive charge onto the metal vertex, but also a larger HOMO-LUMO gap [12]. Schilling and Hoffmann also suggested that the favored pathway is the antarafacial migration depicted in Fig. 1; this route stabilizes the transition state by interaction of the p orbital on the migrating methylene with an out-of-phase combination of metal d_{z^2} orbitals [11].

These concepts have been extended to the closely analogous $[(RC{\equiv}C{-}CR'R'')]^+$ cations, **2**, whose synthetic potential has been brilliantly exploited by Nicholas [13] and by Schreiber et al. [14]. Although no crystallographic data have been reported on these cobalt-stabilized cations, Edidin et al. [15] have provided compelling NMR evidence in favor of the C_s isomer **1a**. Moreover, the mixed-metal cluster **3**, which is the isoelectronic analogue of **2**, has very recently been crystallographically characterized [16].

It is noteworthy that the antarafacial migration process shown in Fig. 1 maintains the identity of the exo and endo substituents at C_α but equilibrates the metal sites. This latter aspect is beautifully illustrated in the $[(C_5H_4Me)_2Mo_2(CO)_4{-}(HC{\equiv}C{-}CH_2)]^+$ cation, **4**, whereby the tricarbonylcobalt moieties in **2** have been replaced by isolobal (cyclopentadienyl)dicarbonylmolybdenum vertices [17]. Curtis demonstrated that the cyclopentadienyl ligands in **4** are equilibrated via a process with an activation energy of ≈ 17 kcal mol^{-1}; in contrast, the barrier for interconversion of the exo and endo α-CH_2 protons is considerably higher [17]. These data are entirely in accord with the antarafacial mechanism depicted in Fig. 1. Subsequent investigations have revealed that the barrier to these antarafacial migrations of α-CR_2^+ fragments from one metal vertex to the other is critically dependent on the primary, secondary or tertiary character of the carbocationic center [18–22]. The activation energy for such a process in molybdenum-, tungsten- or cobalt-stabilized α-CR_2^+ moieties falls from ≈ 18 kcal mol^{-1} for 1° cations to ≈ 10 kcal mol^{-1} for 3° cations, indicating that the more stable tertiary centers have much less need for anchimeric assistance from the metal than do primary cations. This apparent weakening of the metal-to-carbocation interaction is also reflected in the increasing Mo···C^+ distances which range from 2.44 Å to 2.74 Å in the series M–CH_2^+, M–CHR^+, M–CR_2^+ [23–30]. These observations prompted us to assemble the available X-ray crystallographic data on the molybdenum cations not only to carry out a Bürgi–Dunitz trajectory analysis but also to complement our detailed EHMO investigation of the reaction pathway.

2.2. *Extended Hückel molecular orbital calculations on Mo_2C_2 cluster cations*

A complicating factor in any calculatory approach to understanding the mechanism of carbocation rearrangement in the $[Cp_2Mo_2(CO)_4(HC{\equiv}C{-}CH_2)]^+$ system is the conformational variability of the $CpMo(CO)_2$ groups as well as the propensity of the carbonyl ligands to adopt semi-bridging positions [31–33]. (The question of the favored orientations of (cyclopentadienyl)dicarbonylmolybdenum vertices has been discussed elsewhere [34].) These difficulties are obviated by taking advantage of Vollhardt's report of the fulvalene complex $[\eta^5 : \eta^5\text{-}(C_5H_4{-}C_5H_4){-}Mo_2(CO)_4(MeC{\equiv}C{-}CH_2)]^+$, **5** [25]. In this relatively rigid bridged biscyclopentadienyl system, the carbonyls are clearly terminal and the structure can justifiably be idealized to the C_s structure. It is this model which we have used for our calculations.

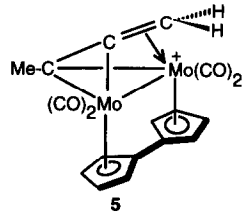

5

In order to define the geometry of the cationic cluster which undergoes rearrangement, we place the origin, ◎, of our coordinate system at the centroid of the Mo(1)–Mo(2)–C(3) basal triangle. The capping carbynyl atom C(2) is defined by a vector starting at the origin and which makes an angle of 71° with the line C(3)–◎. The distance C(3)–C(2) was taken as 1.369 Å, as in **5**. The coordinates of the α-CH_2 unit are defined

in terms of the C(2)–C(1) distance (1.475 Å) and the three angles θ, ϕ and ω. As shown in Fig. 2, θ is the angle ◎–C(2)–C(1) which decreases from 180° as the methylene unit is allowed to lean towards the Mo(1)–Mo(2) bond. As the methylene group swivels away from the mirror plane which contains C(3) and C(2), the dihedral angle ϕ opens up from 0° towards 70° at which point the C(2)–C(1) bond eclipses the C(2)–Mo(1) vector. The third degree of freedom, the twist angle ω, defines the positions of the hydrogens attached to C(1). When all three components of the CH_2 unit lie in the molecular mirror plane ($\phi = 0°$) the ω values are 0° for H_{endo} and 180° for H_{exo}. As the methylene fragment swivels towards Mo(1), one might anticipate that the values $\omega(H_{endo})$ and $\omega(H_{exo})$ would gradually evolve towards 90° and −90°, respectively. To generate the hypersurface shown in Fig. 3, the angles θ and ϕ were incremented in units of 5° and 2°, respectively. At each point the torsion angle ω was varied from 0° to 180° in 15° increments and the minimum energy ω value for each (θ,ϕ) position was plotted.

We see that at $\phi = 0$ the molecule maintains C_s symmetry such that the p orbital at C(1) is oriented parallel to the Mo–Mo axis. This geometry optimizes the overlap of the vacant orbital of the cationic carbon

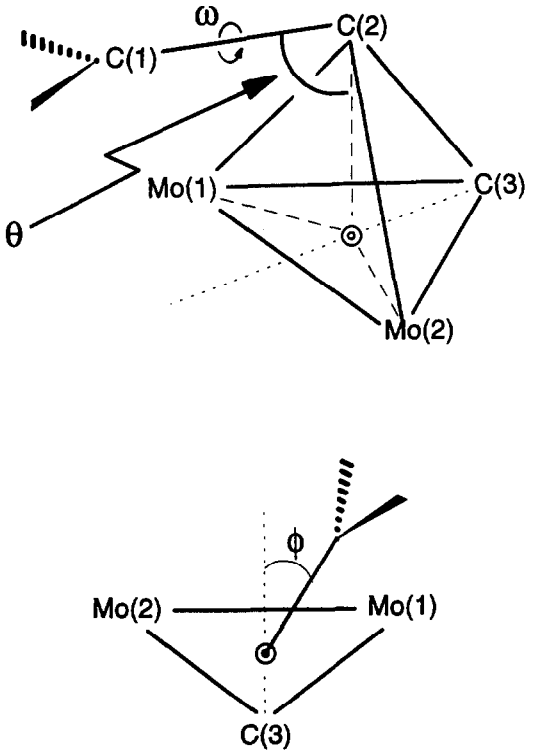

Fig. 2. Definition of the angles θ, ϕ and ω which define C(1) and C(2).

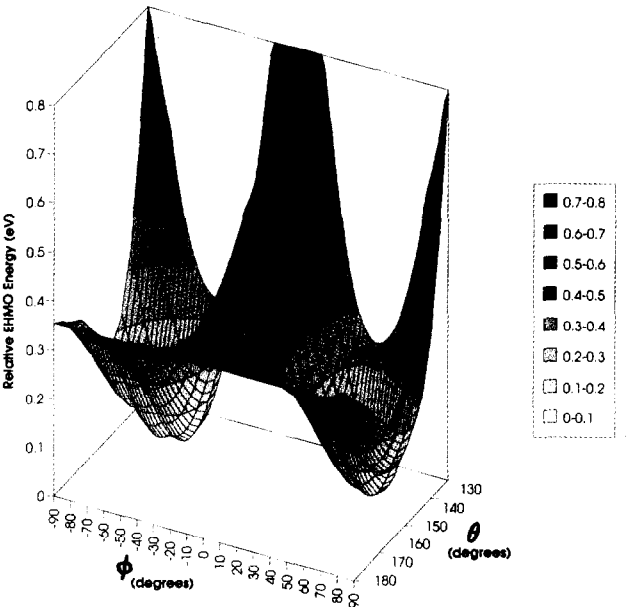

Fig. 3. Energy hypersurface for the migration of the CH_2 group in $[\eta^5:\eta^5\text{-}(C_5H_4\text{–}C_5H_4)Mo_2(CO)_4(HC{\equiv}C\text{–}CH_2)]^+$.

with the filled d_{z^2} orbitals on both metals and so stabilizes the electron-deficient methylene center during its transit from one molybdenum vertex to the other. The optimal value of the bend angle θ is 175°, i.e. the CH_2 group leans only slightly towards the Mo–Mo vector. As ϕ increases to 20°, the initially relatively flat region of the hypersurface begins a precipitous drop into a potential well. This fall is accompanied by a sharp decrease in θ, the ◎–C(2)–C(1) bend angle, which becomes 140° by the time ϕ reaches 28°. The value of θ remains essentially constant as one approaches the global minimum, and indeed is maintained briefly even after the C(2)–C(1) bond has passed the $\phi = 70°$ mark, corresponding to the eclipsing of the C(2)–Mo(1) vector.

The global minimum is located in the region $\phi = 50°$ to 70°, where the energy is virtually constant. Careful scrutiny of the potential well, shown in Fig. 3, reveals a small fluctuation at the bottom of the well; this is reflected as the calculated global minimum at $\phi = 54°$, with a subtly differentiated local minimum at $\phi = 62°$. Of course, such observations may be attributable to artifacts of the EHMO calculation and may disappear at a higher level of approximation but, as we shall see in the discussion of the X-ray diffraction data, a number of cations of this type crystallize with two noticeably different structures in the same unit cell.

The orientation of the hydrogen atoms of the migrating group, as indicated by the torsional angle ω, was found to evolve with increasing ϕ so as to allow an optimal interaction of the carbon p orbital with the

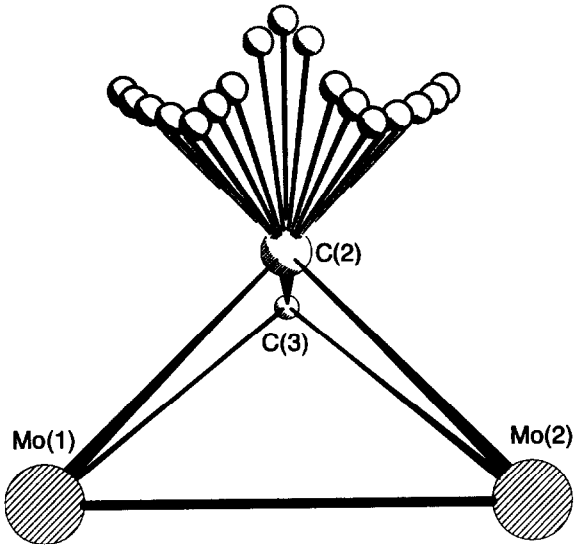

Fig. 4. View of the EHMO-calculated trajectory of C(1) during the migration process.

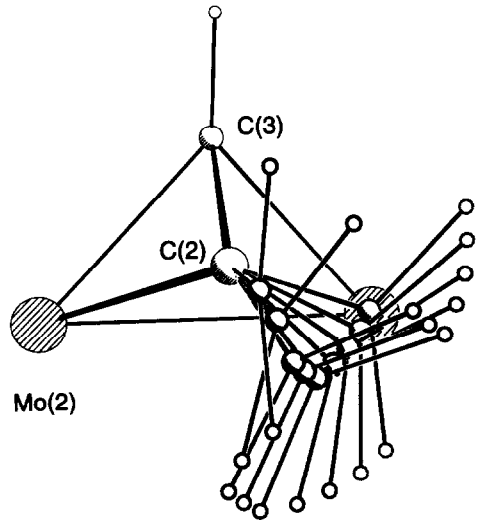

Fig. 5. Bird's eye view of the EHMO-calculated twisting motion of the CH_2 fragment during the migration process.

filled d orbital on the molybdenum atom towards which it is moving. In order to compute the lowest-energy pathway for migration of C(1) from Mo(1) to Mo(2), we used the data embedded in Fig. 3 to seek out, for each value of ϕ, the optimal value of θ. The (θ,ϕ) coordinates thus obtained were then further refined in terms of ω, at a resolution of 2°, to reveal the pathway depicted in Figs. 4 and 5. The former shows the calculated trajectory followed by C(1), and the character of the rather steep descent into the potential well near each molybdenum is evident. The EHMO-calculated barrier for a methylene cation migrating from one molybdenum site to the other is 9 kcal mol^{-1}, somewhat lower than the experimentally determined activation energy. However, we note that our chosen model, with its idealized C_s tetrahedral core and bridging $\eta^5:\eta^5$-$(C_5H_4–C_5H_4)$ fragment, takes no account of the energy required to deform the relatively rigid fulvalene ligand. Nevertheless, calculations based on the linked bis-cyclopentadienyl system **5** avoid the complications of $CpMo(CO)_2$ vertex rotations and exchange of terminal and semi-bridging carbonyls.

Fig. 5 illustrates the evolution of the methylene twist angle ω as the migrating fragment seeks to maximize its orbital overlap with molybdenum as it approaches the metal center. Thus, the plane containing C(1) and its attached hydrogens rotates relative to the Mo(1)–Mo(2)–C(3) basal triangle such that, when $\phi = 0°$, these two planes are orthogonal but, at $\phi = 70°$, they are almost parallel.

2.3. *Musical interlude*

We digress for one moment to draw attention to the observation that this pathway for methylene migration

TABLE 1. Crystallographic data for molybdenum cations

Structure	rMo(1)–C(1) (Å)	r◎–C(2) (Å)	∠C(3)–◎–C(2)(°)	rC(2)–C(1) Å)	θ ◎–C(2)–C(1)(°)	ϕ C(3)–◎–C(2)–C(1) (°)	Ref.
$[(C_5H_4\text{-}C_5H_4)Mo_2(CO)_4(MeC{\equiv}C\text{-}CH_2)]^+$	2.442	1.248	71.3	1.475	123	61	[25]
$[(C_5H_5)_2Mo_2(CO)_4(HC{\equiv}C\text{-}CH_2)]^+$	2.444	1.315	68.3	1.379	122	58	[24]
$[(C_5H_4Me)_2Mo_2(CO)_4(HC{\equiv}C\text{-}CH_2)]^+$	2.465	1.358	67.0	1.345	124	53	[17]
$[(C_5H_4Me)_2Mo_2(CO)_4(HC{\equiv}C\text{-}CH_2)]^+$	2.468	1.324	69.0	1.437	122	53	[17]
$[(C_5H_4\text{-}C_5H_4)Mo_2(CO)_4(MeC{\equiv}C\text{-}CH_2)]^+$	2.557	1.251	70.9	1.484	128	51	[25]
$[(C_5H_5)_2Mo_2(CO)_4(HC{\equiv}C\text{-}CHMe)]^+$	2.613	1.354	70.7	1.380	132	72	[26]
$[(C_5H_5)_2Mo_2(CO)_4(BuC{\equiv}C\text{-}CH(ferrocenyl))]^+$	2.630	1.316	68.4	1.424	123	54	[28]
$[(C_5H_5)_2Mo_2(CO)_4(MeC{\equiv}C\text{-}bornyl)]^+$	2.737	1.350	65.1	1.397	136	50	[30]
$[(C_5H_5)_2Mo_2(CO)_4(HC{\equiv}C\text{-}mestranyl)]^+$	2.738	1.368	66.5	1.364	127	53	[29]
$[(C_5H_4\text{-}C_5H_4)Mo_2(CO)_4(HC{\equiv}C\text{-}CMe_2)]^+$	2.753	1.404	68.7	1.361	126	71	[27]
$[(C_5H_5)Mo(CO)_2Co(CO)_3(MeC{\equiv}C\text{-}bornyl)]^+$	2.915	1.350	65.1	1.397	146	50	[30]

is remarkably similar to the trajectory followed by a conductor's baton during an orchestral performance. This phenomenon is dramatically and beautifully illustrated in Fig. 6.

2.4. X-ray crystallographic data for Mo_2C_2 cluster cations

The establishment of a trajectory for migration of the CR_2^+ moiety between metal vertices requires the compilation of a series of X-ray crystal structures of the $[Cp_2Mo_2(CO)_4(RC{\equiv}C{-}CR'R'')]^+$ type. Data are available for the cations listed in Table 1, and include such R', R'' substituents as H [17,23–25], methyl [26,27] and ferrocenyl [28], as well as steroidal [29] and terpenoid [30] fragments. We see from Table 1 that, as noted previously, the $Mo\cdots C^+$ distances lengthen as the character of C(1) changes from a primary carbon, to a secondary carbon, and finally to a tertiary cationic center. However, for the present purpose, we need to know not only bond distances but also the experimental values of the bend angle θ, and the torsional parameters, ϕ and ω, for each cationic cluster. Analogously to the method used for the EHMO calculations, the origin, ◎, was defined as the centroid of the Mo(1)–Mo(2)–C(3) triangle; the distances ◎–C(2) and C(2)–C(1), and the angles C(3)–◎–C(2), θ, ϕ, and ω, were evaluated from the X-ray crystallographic data. These measurements yielded cartesian coordinates for the C(2) and C(1) atoms, as well as for any non-hydrogen substituents attached to C(1). In Fig. 7, the C(2) and C(1) positions for each of the eleven crystallographically determined structures are superimposed on the Mo_2C triangular base of **5**. This allows a direct

Fig. 6. Multiple exposure flash photographs of Akira Endo conducting the Hamilton Symphony Orchestra in a performance of Tchaikovsky's 6th Symphony.

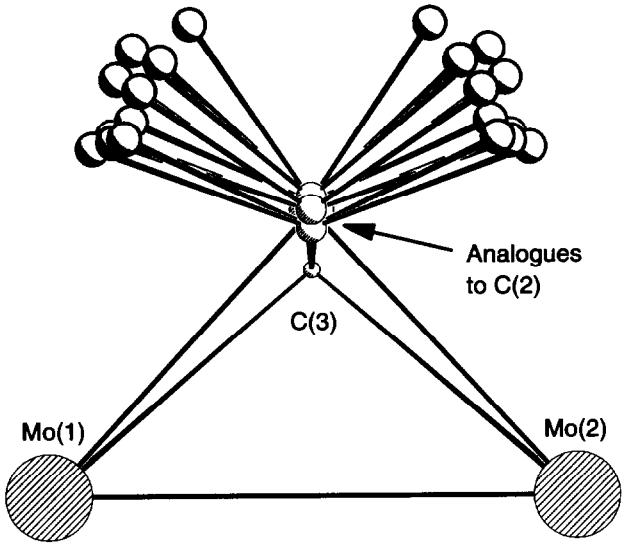

Fig. 7. Superposition of the C(1) cationic centers in 11 different X-ray crystal structures, $[Cp_2Mo_2(CO)_4(RC{\equiv}C{-}CR'R'')]^+$.

comparison with the atomic positions for the EHMO-calculated minimum energy pathway shown in Figs. 4 and 5.

It is immediately apparent from a comparison of Figs. 4 and 5 with Figs. 7 and 8, respectively, that there is an excellent correlation between the EHMO-calculated and X-ray determined series of structures. The crystallographically located positions of the C(2) capping carbons in the series of clusters, although very similar, are not identical, showing that one can consider the whole vinylidene fragment to be capable of moving over the triangular base. Nevertheless, it is evident that the locus of the cationic site is readily defined in terms of the angles θ and ϕ.

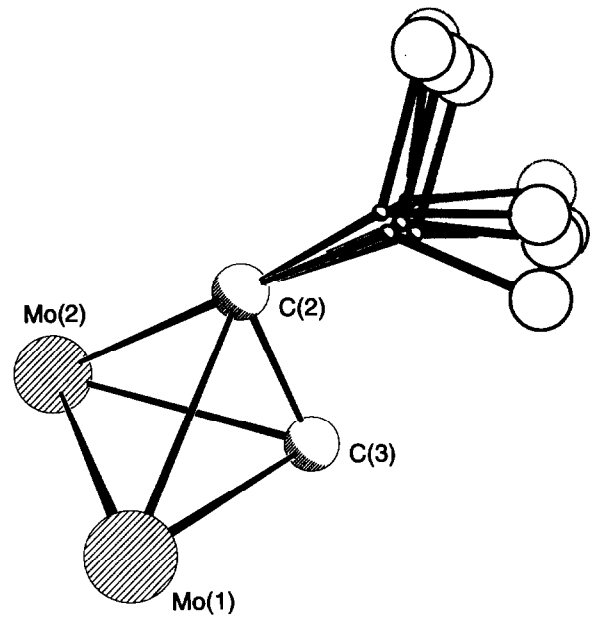

Fig. 8. View of the twisting motion of the CR'R'' fragment in a series of X-ray crystal structures.

It is fortunate that the $[Cp_2Mo_2(CO)_4(RC{\equiv}C{-}CR'R'')]^+$ clusters whose structures have been reported cover a range of substituents with widely differing electronic and steric requirements, and so yield a data set with bend angles, θ, varying from 122° to 146° and with torsional angles, ϕ, covering the range 50° to 70°. These values encompass almost the entire domain of the deep potential well in the hypersurface depicted in Fig. 3. Indeed, one can clearly see that the tertiary cationic centers have not merely lengthened the Mo $\cdots$ C^+ distances relative to those found in CH_2^+ systems, but have also started to climb out of the potential well by rotating the C(2)–C(1) vector towards the mirror plane which bisects the two molybdenum vertices. Moreover, as illustrated in Fig. 8, the twist angles ω gradually evolve such that the exo and endo substituents move towards their predicted vertical positions as the migration proceeds. We note also that, in those crystal structures where the substituents attached to C(1) are observable, the cationic center is not planar in an ideal sp^2 fashion, but rather shows a tendency to pyramidalize. Of course, in those cases where the greatest pyramidalization is to be expected, i.e. with the primary cations most firmly bonded to the metal center, the α-hydrogens cannot be located unequivocally. Interestingly, the EHMO calculations suggest that, at the calculated global minimum energy for **5** (where $\theta = 140°$ and $\phi = 54°$), the methylene hydrogens can each be bent away from the Mo atom by 8°; this stabilizes the system to the tune of ≈ 1.2 kcal mol^{-1}.

Finally, we find it noteworthy that in two of the systems studied, namely $[(C_5H_4Me)_2Mo_2(CO)_4(HC{\equiv}C{-}CH_2)]^+$, **4**, and $[\eta^5{:}\eta^5\text{-}(C_5H_4{-}C_5H_4)Mo_2(CO)_4(MeC{\equiv}C{-}CH_2)]^+$, **5**, there are two independent molecules of the cation in the unit cell. In each case, this effect manifests itself as a slightly different orientation of the methylene fragment with respect to the nearby molybdenum vertex. In **5**, the Mo $\cdots$ C^+ distances in the two molecules are 2.44 Å and 2.56 Å and, while these may possibly be dismissed simply as crystal packing effects, one might also consider that this phenomenon reflects the observation of two calculated minima, as shown in Fig. 3. Clearly, we are close to the limits of reliability of the EHMO approach but, nevertheless, it provides food for thought!

3. Conclusions

In summary, the remarkable similarity of the calculated lowest-energy pathway for cation migration be-

tween two metal vertices, and the trajectory indicated by a series of crystallographic "snapshots" of the process is manifest evidence of the power of the Bürgi-Dunitz approach towards understanding molecular dynamics. According to the basic assumptions of the structure correlation method [1], there should be a concentration of sample points (i.e. crystal structures) in the low-energy regions of three-dimensional space. Moreover, there should be a gradual thinning-out of sample points along the reaction path as the energy rises. One may thus identify the transition state as lying in the least densely populated stretch of the reaction path. In the present case, this is when the angle ϕ approaches 0° and the plane containing the CH_2 moiety is orthogonal to the basal plane of the tetrahedral cluster.

We suggest that the complete characterization of a fluxional process, observed for a series of related molecules, requires not only an NMR investigation but also molecular orbital calculations complemented by a trajectory analysis of the available X-ray structural data. The ready accessibility of crystallographic databases, coupled with the ever-increasing power of personal computers, will soon render such endeavors routine.

4. Computational methods

Molecular orbital calculations were performed within the extended Hückel formalism using weighted H_{ij} values [35–37]. Computations were carried out by use of the program CACAO [38] on an EVERDATA 486 50 MHz IBM clone which required ≈ 84 h to generate the data from which the surface shown in Fig. 3 was constructed. Microsoft EXCEL 4.0's "Chart Wizard" was used to generate the 3D surface as a mesh plot.

Acknowledgements

Financial support from the Natural Sciences and Engineering Research Council of Canada is gratefully acknowledged. We thank Professor G. Jaouen and his colleagues in Paris for many valuable discussions. Finally we are grateful to the Editor of the *Hamilton Spectator* for permission to reproduce Fig. 6.

References

1 H.B. Bürgi and J.D. Dunitz, *Acc. Chem. Res., 16* (1983) 153.
2 H.B. Burgi, J.D. Dunitz and E. Shefter, *J. Am. Chem. Soc., 95* (1973) 5065.
3 J.E. Baldwin, *J. Chem. Soc., Chem. Commun.*, (1976) 734.
4 E. Bye, W.B. Schweizer and J.D. Dunitz, *J. Am. Chem. Soc., 104* (1982) 5893.
5 D. Gust and K. Mislow, *J. Am. Chem. Soc., 95* (1973) 1535.
6 J.F. Blount, P. Finocchiaro, D. Gust and K. Mislow, *J. Am. Chem. Soc., 95* (1973) 7019.
7 J.D. Andose and K. Mislow, *J. Am. Chem. Soc., 96* (1974) 2168.
8 K. Mislow, *Acc. Chem. Res., 9* (1976) 26.
9 R.H. Crabtree and M. Lavin, *Inorg. Chem., 25* (1986) 805.
10 D. Seyferth, *Adv. Organomet Chem., 14* (1976) 97.
11 B.E.R. Schilling and R. Hoffmann, *J. Am. Chem. Soc., 101* (1979) 3456.
12 M.F. D'Agostino, M. Mlekuz, J.W. Kolis, B.G. Sayer, C.A. Rodger, J.-F. Halet, J.-Y. Saillard and M.J. McGlinchey *Organometallics, 5* (1986) 2345.
13 K.M. Nicholas, *Acc. Chem. Res., 20* (1986) 207.
14 S.L. Schreiber, M.T. Klimas and S. Sammakia, *J. Am. Chem. Soc., 109* (1987) 5749.
15 R.T. Edidin, J.R. Norton and K. Mislow, *Organometallics, 1* (1982) 561.
16 D. Osella, G. Dutto, G. Jaouen, A. Vessières, P.R. Raithby, L. De Benedetto and M.J. McGlinchey, *Organometallics, 12* (1993) 4545.
17 A. Meyer, D.J. McCabe and M.D. Curtis, *Organometallics, 6* (1987) 1491.
18 V.I. Solokov, I.V. Barinov and O.A. Reutov, *Isv. Akad. Nauk SSR, Ser. Khim.*, (1982) 1922.
19 S. Padmanabhan and K.M. Nicholas, *J. Organomet. Chem., 268* (1983) C23.
20 S.F.T. Froom, M. Green, K.R. Nagle and D.J. Williams, *J. Chem. Soc., Chem. Commun.*, (1987) 1305.
21 M.V. Galakhov, V.I. Bakhmutov, I.V. Barinov and D.A. Reutov, *J. Organomet. Chem., 421* (1991) 65.
22 C. Cordier, M. Gruselle, G. Jaouen, V.I. Bakhmutov, M.V. Galakhov, L.L. Troitskaya and V.I. Solokov, *Organometallics, 10* (1991) 2303.
23 I.V. Barinov, O.A. Reutov, A.V. Polyakov, A.L. Yanovsky, Yu. T. Struchkov and V.I. Sokolov, *J. Organomet. Chem., 418* 1991, C24.
24 C. Cordier, *Ph.D. Thesis*, Université Pierre et Marie Curie, Paris, 1991.
25 H. El Amouri, J. Vaissermann, Y. Besace, K.P.C. Vollhardt and G.E. Ball, *Organometallics, 12* (1993) 605.
26 N. Leberre-Cosquer, R. Kergoat and P. L'Haridon, *Organometallics, 11* (1992) 721.
27 H. El Amouri, Y. Besace, J. Vaissermann, M.J. McGlinchey and G. Jaouen, *Organometallics,* submitted.
28 C. Cordier, M. Gruselle, J. Vaissermann, L.L. Troitskaya, V.I. Bakhmutov, V.I. Sokolov and G. Jaouen, *Organometallics, 11* (1992) 3825.
29 M. Gruselle, C. Cordier, M. Salmain, H. El Amouri, C. Guérin, J. Vaissermann and G. Jaouen, *Organometallics, 9* (1990) 2993.
30 M. Gruselle, H. El Hafa, M. Nikolski, G. Jaouen, J. Vaissermann, L. Li and M.J. McGlinchey, *Organometallics, 12* (1993) 4917.
31 W.I. Bailey, Jr., M.H. Chisholm, F.A. Cotton and L.A. Rankel, *J. Am. Chem. Soc., 100* (1978) 5764.
32 P. Bougeard, S. Peng, M. Mlekuz and M.J. McGlinchey, *J. Organomet. Chem., 296* (1985) 386 (and references therein).
33 G.A. Carriedo, J.A.K. Howard, D.B. Lewis, G.E. Lewis and F.G.A. Stone, *J. Chem. Soc., Dalton Trans.*, (1985) 905.
34 S. Tondu, G. Jaouen, M.F. D'Agostino, K.L. Malisza and M.J. McGlinchey, *Can. J. Chem., 70* (1992) 1743.
35 R. Hoffmann, *J. Chem. Phys., 39* (1963) 1397.
36 R. Hoffmann and W.N. Lipscomb, *J. Chem. Phys., 36* (1962) 2179, 3489.
37 J.H. Ammeter, H.B. Bürgi, J.C. Thibeault and R. Hoffmann, *J. Am. Chem. Soc., 100* (1978) 3686.
38 C. Mealli and D.M. Proserpio, *J. Chem. Educ., 67* (1990) 3399.